IOP PUBLISHING JOURNAL OF PHYSICS D: APPLIED PHYSICS
J. Phys. D: Appl. Phys. **41** (2008) 205204 (9pp) doi:10.1088/0022-3727/41/20/205204

Prospects of airflow control by a gliding arc in a static magnetic field

N Balcon[1], N Benard[1], P Braud[1], A Mizuno[2], G Touchard[1] and E Moreau[1]

[1]Laboratoire d'Etudes Aérodynamiques (LEA), Université de Poitiers, ENSMA, CNRS B[ld] Marie et Pierre Curie, Téléport 2, 86962 Futuroscope Cedex, France
[2] Toyohashi University of Technology, Japan, Hibarigaoka, Tempaku-cho, Toyoashi, Aichi 441-8580, Japan

Received 1 August 2008, in final form 28 August 2008
Published 25 September 2008
Online at stacks.iop.org/JPhysD/41/205204

Abstract
The electrical properties of a gliding arc operating in air at atmospheric pressure are studied to evaluate its possible applications to flow control. The electromechanical behaviour of the discharge travelling at 4 m s^{-1} along diverging electrodes in a static magnetic field is analysed in detail. Two different methods are proposed to evaluate the velocity of the arc. An initial estimation is based on the arc current evolution during its transit and additional information is gained from fast digital imaging with a CCD camera. The displacement of the arc observed with short exposure time corroborates the electrical measurement and also exhibits the existence of luminous points on the cathode that can slow down the arc motion. In addition, a particle image velocimetry system is used to investigate the interaction between the gliding arc and the surrounding air. The displacement of the low current glidarc creates a low velocity convection (around 0.2 m s^{-1}) in the gas and also generate faster structures up to 1 m s^{-1} directly in front of the discharge. These electromechanical effects could be used to manipulate the boundary layer region of various aerodynamic shapes.

(Some figures in this article are in colour only in the electronic version)

1. Introduction

The control of airflows by electrical discharges in various configurations has attracted an increasing amount of interest in the past decade and is still the subject of numerous investigations. Compared with other actuators such as micro-electro-mechanical actuators (MEMs) or blowing jets, electrical discharge based actuators bring momentum to the flow without the injection of additional mass. These actuators, free of mechanical parts, have a time response much greater than MEM and are thus very well adapted to real-time closed loop control. Moreover, this short time response allows one to amplify or cancel the instabilities of airflows by acting on the natural frequency of Kelvin–Helmholtz or Tollmien–Schlichting waves. Several experiments and theoretical studies have demonstrated the efficiency of electro-magneto hydrodynamic (EMHD) effects for flow control over a wide range of velocities [1–5]. The possible applications of dielectric barrier discharge (DBD) actuators have been reported by many authors as reviewed in [6, 7]. They are suitable especially for airfoils, cylinders and flat plate configuration [8–20]. Other electrical discharges such as arcs have been proven to heat the gas and generate strong compression waves [21] and also to affect the boundary layer [22]. Thus they are versatile for airflow control in many configurations. Significant effects have been observed when arc discharges are placed at the exit of jet nozzles. In particular, the mixing properties [23, 24] and the broadband noise level [25] can be efficiently controlled. The possibility of manipulating scramjet inlets by operating near surface arcs has been demonstrated [26, 27]. Experimental results have also proven that low current arcs can be stabilized in airflow and be used for microwave attenuation [28].

When immersed in a static external magnetic field the displacement of an electric arc can be controlled. The effectiveness of this process for circuit breakers has been numerically investigated and reported in [29]. Gliding arcs are also effective in pollution control in various gases [30–32]. In this paper we focus on the electrical and mechanical properties of a gliding arc operating in still air. Our objective is to test and characterize the motion and the effects on the gas of a low current electric arc (30 mA) travelling in a magnetic

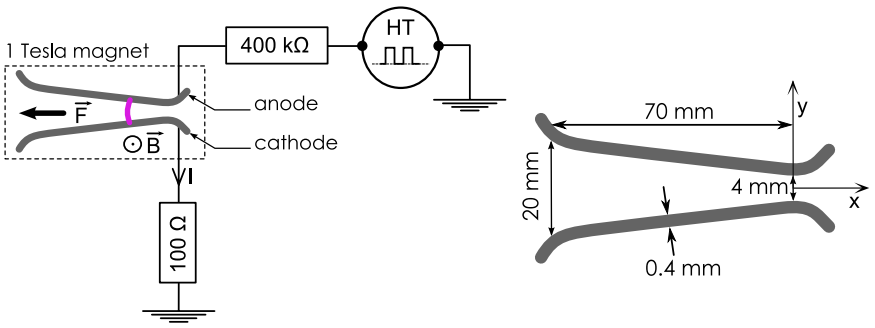

Figure 1. Glidarc experimental configuration with diverging electrodes and permanent magnet.

field of approximately 0.8 T (1 mm above a 1 T magnet). The influence of the electrode configuration is also reported. Finally, the effects of the discharge on the surrounding air have been witnessed and quantified by means of a particle image velocimetry (PIV) apparatus. This kind of low current arc can locally heat the gas and create expansion regions following its movement without damaging the surface. Hence it could present relevant insights into future applications in airflow control over a range of velocities wider than EFD actuators that operate without a magnetic field.

2. Experimental configuration

A gliding arc (glidarc) is created by a pulsed dc voltage with an amplitude varying between 1 and 7 kV applied across two diverging electrodes made of copper wire (0.4 mm of diameter, see figure 1). A high voltage amplifier (Trek, 40 mA/20 kV) controlled by a programmable signal generator (TTI, TG1010A) delivers positive pulses at a frequency of 10 Hz with 50% duty cycle. A 400 kΩ resistance protects the generator from too high currents peaks. The potential on the anode is measured with a high voltage probe (North Star, PVM-1 1 : 1000). A low 100 Ω resistor is placed between the cathode and the ground in order to measure the current running through the circuit. The voltage across this resistor is measured with a digital oscilloscope (Tektronix 3014—100 MHz bandwith). The set of electrodes is mounted over a neodymium–iron–boron permanent magnet (80 mm × 20 mm) producing a static magnetic field of 1 T perpendicular to the surface (approximately 0.8 T 1 mm above the dielectric). In order to prevent an electric discharge from taking place between the anode and the magnet a 1 mm layer of mica, acting as a dielectric, is inserted between them. This set-up is embedded onto a poly-methyl-meth-acrylate (PMMA) flat plate (2 cm × 14 cm × 20 cm).

The ignition always takes place where the inter-electrode spacing is the shortest (4 mm). Then the arc which acts as a charged particle channel experiences the macroscopic Laplace force proportional to the cross product $\boldsymbol{I} \times \boldsymbol{B}$, where $\boldsymbol{I}$ and $\boldsymbol{B}$ are, respectively, the current and magnetic field amplitude. This results in the displacement of the arc all along the electrodes' length (70 mm) in the direction of increasing gap size (always from right to left as shown in figure 1). When the arc becomes longer its resistance increases and the current is reduced. Above a certain threshold (when the arc is approximately 20 mm long) the arc eventually breaks and starts again at the ignition point. Hence the transit of the arc always occurs in the same direction. The velocity of the arc is deduced from the electrical curves and also from the acquisition of digital images at a high repetitive rate. A CCD camera with a 1024 × 256 pixels resolution running at 10 kHz captures images of the glidarc on an axis view perpendicular to the surface (see figure 1 for the definition of the coordinate system). A windowed spatial cross correlation between successive images allows us to measure the arc velocity in details. Additionally to these electrical and optical measurements, the interaction between the surrounding air and the glidarc is studied by PIV (set-up sketched in figure 2).

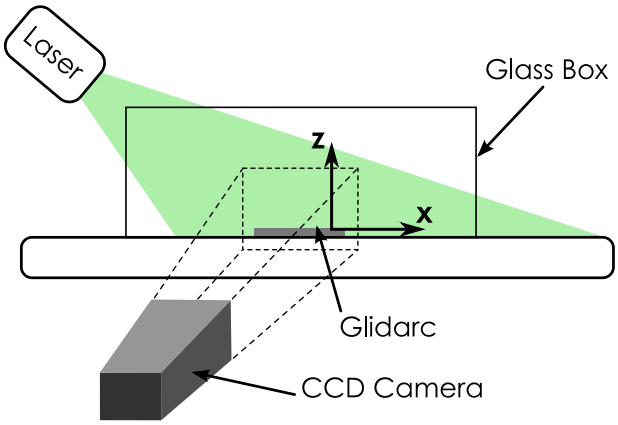

Figure 2. PIV apparatus (green light sheet perpendicular to the surface and parallel to the arc displacement).

3. Electrical properties

The applied signal is periodic with a pulse frequency of 10 Hz allowing the arc to cover the total electrode length approximately three times during a 50 ms pulse. As the arc extinction is insured by the diverging set-up, dc excitation is possible. However, considering the power dissipated in the resistor, pulsing the high voltage amplifier is more appropriate in preventing it from overheating. Several excitation frequencies have been tested, from dc signals to 100 kHz. When the pulse width is lower than 5 ms, the arc transit does not cover the entire electrode length. Hence heat generated by the arc is dissipated over a small region of the mica dielectric that can be rapidly damaged.

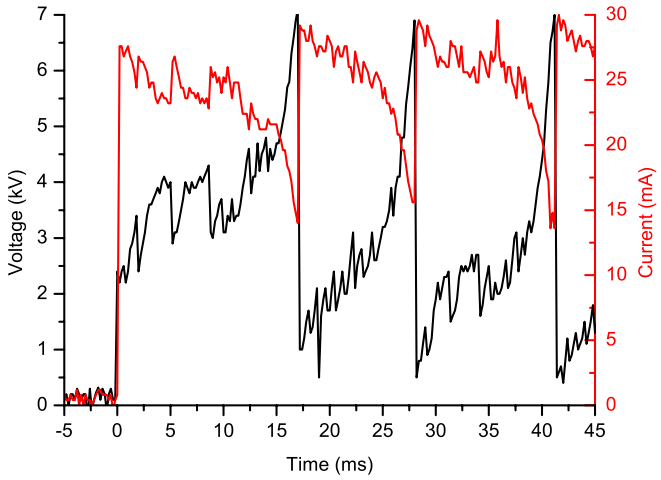

Figure 3. Electrical behaviour of the glidarc during a 50 ms pulse.

As shown in figure 3 for a 50 ms pulse, the temporal evolution of the voltage and current gives a reasonable approximation of the arc time averaged velocity (averaged over the time necessary to cover the entire electrode length). At the beginning of the pulse the applied voltage is approximately 6.5 kV and an arc appears joining the two electrodes. After the ignition of the discharge a conduction current passes through the arc and, combined with the magnetic field, forces it to move and become longer. When the arc length increases, its resistance also increases (from approximately 10 to 500 kΩ), resulting in a lower current and larger voltage. The symmetric evolution of the current and voltage is remarkable. The arc displacement continues until the current becomes lower than the value necessary to sustain a 20 mm arc (approximately 15 mA). When the arc breaks at the end of the pair of electrodes, the whole phenomenon starts over again at the ignition point. The voltage is then sufficient again to ignite another arc. This cyclic behaviour corresponds to the current and voltage evolutions represented in figure 3, where the total time necessary to travel from one end of the electrodes to the other (70 mm) is about 16 ± 3 ms. Hence, the resulting average velocity is approximately 4.3 m s^{-1}. The irregularities in both curves and the variation of the transit time are caused by the arc attachment on the cathode surface and are discussed in the following section.

4. Arc motion observed with high speed digital camera

Fast framing imaging corroborates the mean velocity value found from electrical measurements and, in addition, it gives space–time resolution of this parameter. The displacement of the arc during four cycles is recorded with a Photron (Ultima APX-RS) fast framing camera. The opening of the camera gate is triggered on the pulse generator and the view axis is perpendicular to the surface. This camera can be operated at 3000 full frames per second at 1 mega pixels resolution. Reduced resolutions can be set leading to an acquisition frequency up to 10 kHz. The sequence obtained during one arc transit is composed of 160 images with a gate opening time of 100 μs and a resolution of 1024×256 pixels at a frequency of 10 kHz. Five of these pictures separated by 4 ms are shown in figure 4. Hence the total sequence presented in figure 4 lasts 16 ms. The cathode connected to the ground is situated at the bottom of the picture.

This sequence indicates accurately where the arc ignition and breaking take place and how its shape evolves during the transit. These results also show that electron injection taking place on the cathode surface has a strong tendency to remain attached whereas the anodic end of the arc travels faster in front of this fixation point. The location of the injection point corresponds to the zone where secondary electrons are released from the metallic electrode. This attachment slows the arc motion and generates current loops around the injection point due to the magnetic field as shown in figure 5 (zoom on the arc creating a current loop). Due to its circular shape around the attachment point, the current loop results in a Laplace force which is not directed towards the left, thereby slowing the arc motion.

When the visualization of the current loop is repeated over several transits, it is remarkable that the location of the injection points varies. The phenomenon triggering the arc attachment, which might involve ion bombardment, thermo-ionization and photo-ionization is not reproduced at constant locations. Hence, it is probably not due to microscopic defects of the electrode surface as could be supposed at first sight. In the perspective of airflow control, this arc attachment should be avoided to increase the arc velocity. Current loops not only slow the arc down but also disturb the symmetry of the velocity vector creating movement of charged particles directed towards the cathode as illustrated by the cross correlation applied to the digital images.

A post-treatment algorithm is applied to the images obtained from the high speed camera in order to evaluate the space and time dependence of the arc velocity. The displacement of the glidarc is calculated using a multipass windowed cross-correlation processing. Two successive images are divided into discrete squares of 64×64 pixels. A first estimation of the displacement is then obtained by spatial cross correlation based on the grey levels. A second cross correlation is applied to the initial result with windows reduced to 32×32 pixels. The interrogating windows are overlapped by 50%, which solves the arc velocity every 1.1 mm. Figure 6 shows the variation of the velocity vectors as the arc travels along the electrodes. The sequence was recorded during one arc transit. It demonstrates that the velocity is almost constant during the entire transit at around 4 m s^{-1}. It also reveals that the maximum velocity is reached quasi-immediately after the arc ignition.

Figure 7 represents the velocity in the x direction, y direction and norm summed over four arc transits. The velocity U_x is relatively constant and homogeneous, which contrasts with U_y. Due to the attachment, the velocity in the y direction for points located near the cathode can reach 1.5 m s^{-1} in the anode to cathode direction.

Further investigations are being carried out to find a new electrode geometry and material combined with an appropriate

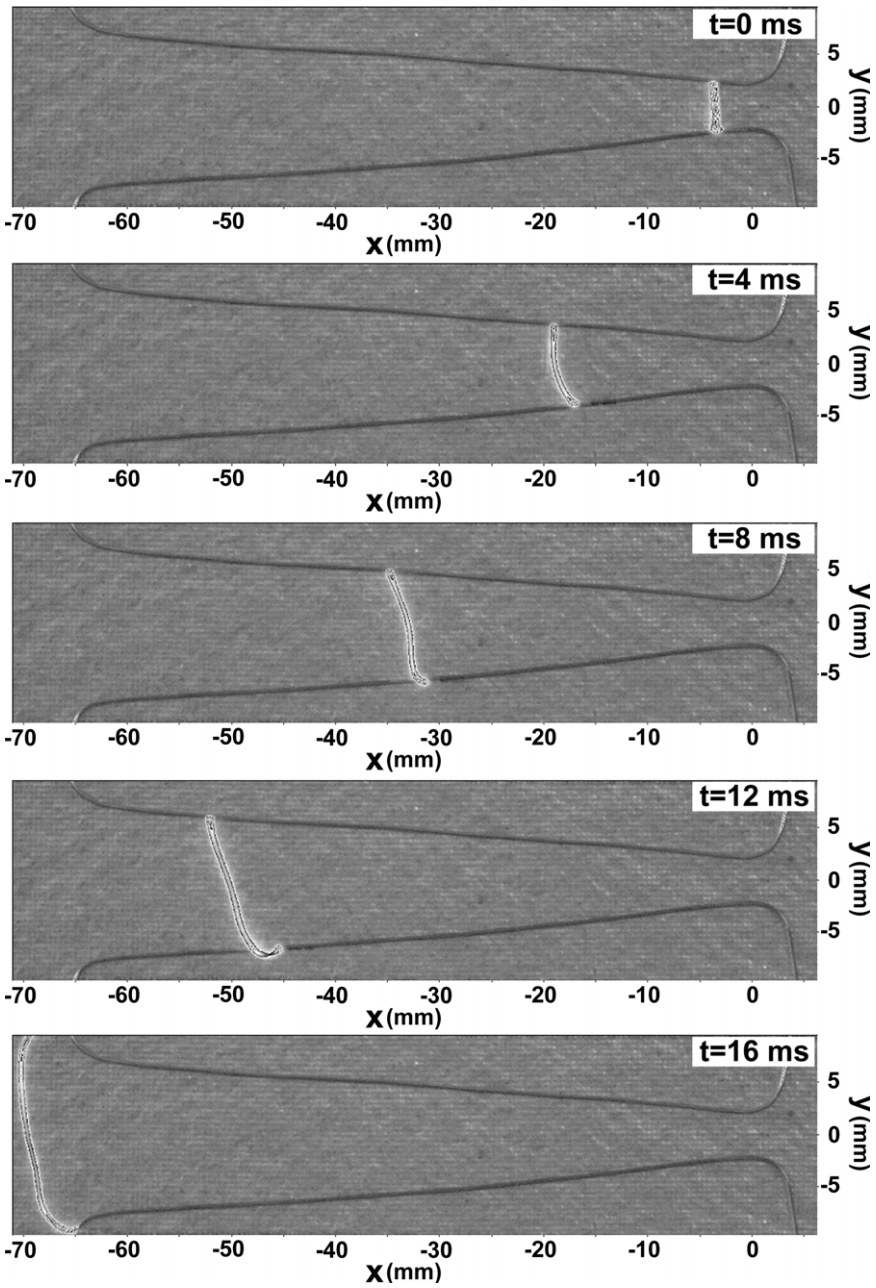

Figure 4. Sequence of four top views (exposure time = 100 μs, 4 ms separate each shot).

magnetic field that would reduce this effect. Without the arc attachment on the cathode, a significant arc velocity increase can be expected. Indeed, a new electrode configuration is currently under investigation. It consists of a circular anode wire around a cathode set-up, as illustrated in figure 8 (The anode loop is 2 cm in diameter and the cathode is a small copper disc 1 mm in diameter). With the same current and magnetic field as in the previous set-up the velocity at the anode end of the arc was measured at 20 m s^{-1} (velocity measured by current analysis). This confirms that without the attachment of the arc on the cathode a greater velocity can be achieved, as illustrated in figure 8. This electrode pair geometry could actually be used for applications where a controllable heat source is required or in surface treatment and pollutant removal systems.

5. Gas/glidarc interaction

The effects of the gliding arc on the surrounding quiescent air have been observed and quantified. It appears that the displacement and the heat of the arc induce a mechanical perturbation on the gas. Evidence of the electromechanical effects are visible with a typical PIV. A Nd : Yag Laser equipped with a cylindrical lens creates a 1 mm thick green light sheet perpendicular to the PMMA flat plate at a frequency of 0.4 Hz. It delivers a power of 27 mJ per pulse. The glidarc set-up is enclosed in a glass box (30 cm × 40 cm × 80 cm) seeded with incense smoke (particle average diameter of 0.3 microns) reflecting the Laser coherent light to the camera objective lens. A Lavision CCD camera captures the 30 mm × 40 mm zone situated over the glidarc with a 1376 × 1040 pixels

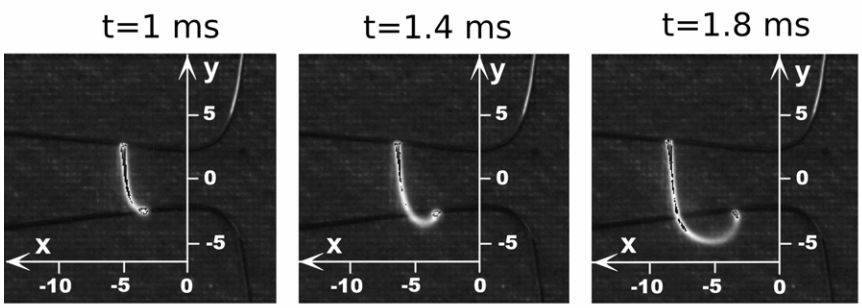

Figure 5. Attachment of the arc on the cathode creating a current loop.

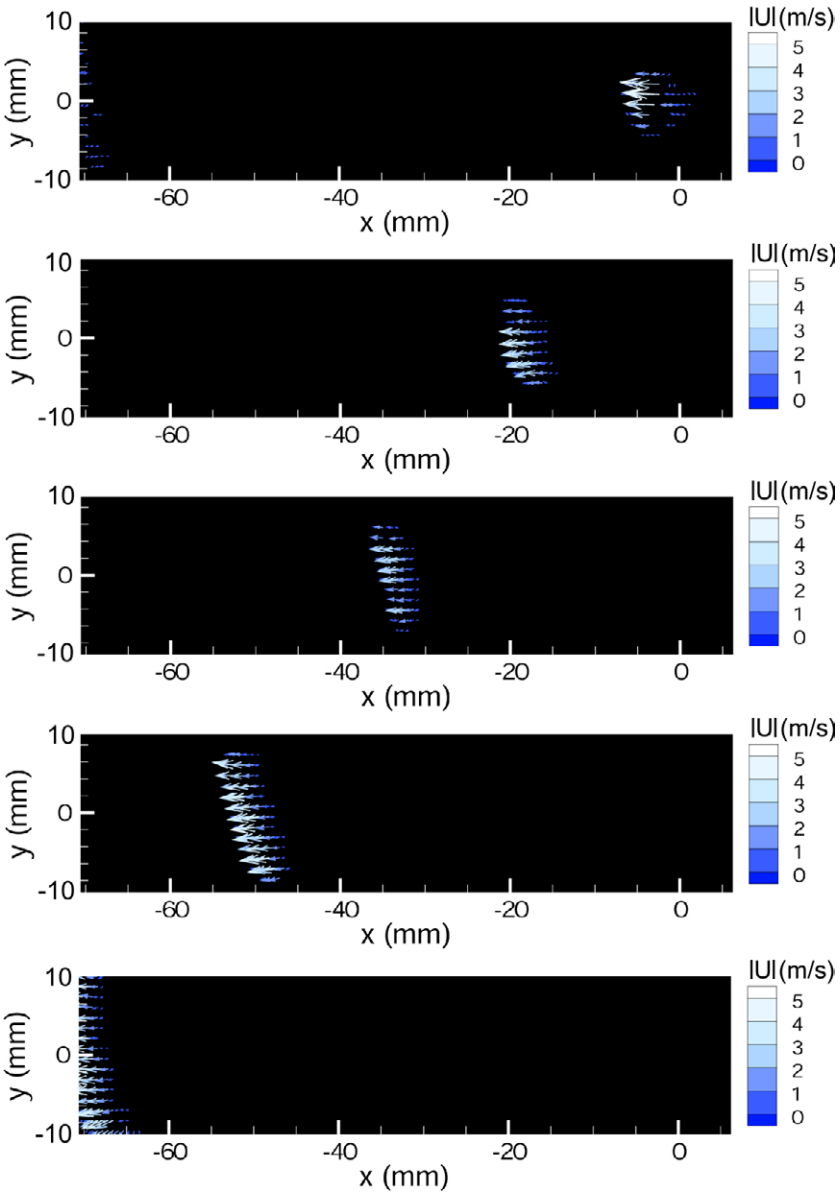

Figure 6. Arc velocity ($\mathrm{m\,s^{-1}}$) at five different positions.

resolution. The aperture of the CCD camera is operated in the dual frame mode. The length of the opening window is adjusted to obtain a displacement of four pixels, which enhances the detection of correlation peaks. The recording frequency is set to 0.4 Hz and 150 pictures are taken for each acquisition. A cross-correlation algorithm with adaptative multipass, interrogation windows of 128×128 to 32×32 pixels and a final overlap set to 50% is applied to the digital couples of images to compute the instantaneous vector fields. The accuracy of the PIV measurement is related to many parameters

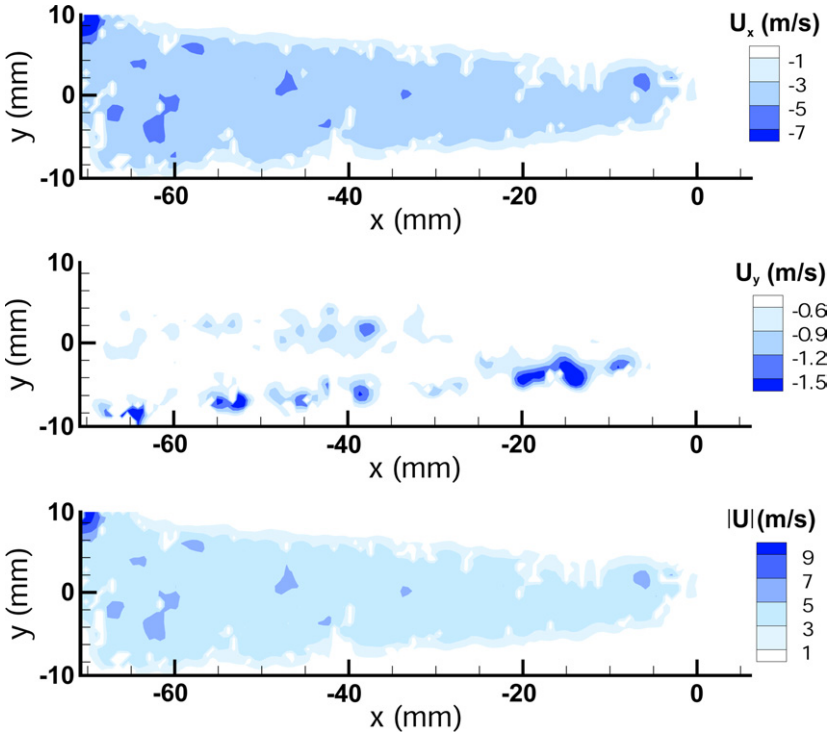

Figure 7. Velocities in the x direction and y direction, norm of the velocity vector ($\mathrm{m\,s^{-1}}$).

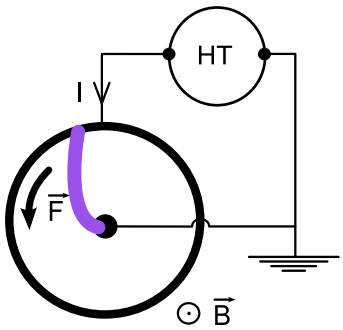

Figure 8. Electrode configuration leading to an arc velocity of $20\,\mathrm{m\,s^{-1}}$ at the anode.

such as particle size, inter-frame time and detection algorithm for instance. A rough estimation of the uncertainty on the measured velocity indicates a maximum relative error level of 2.2%.

In figure 9 the time average velocity vector field (left graph) and norm (right graph) are presented. To clarify the interpretation, only one vector out of two is represented on the vector field in the z direction (see figure 2). The resolution of the PIV apparatus in this configuration is $1.1\,\mathrm{mm} \times 1.1\,\mathrm{mm}$. The average velocity field is calculated over 150 acquisitions which are randomly placed relative to the electric signal. The general movement of the flow is directed upwards with a slight angle towards the left. This is probably due to the combination of the gas heating in the discharge region and to the displacement from the right to the left of the glidarc. The x component of the velocity suggests that the motion of the arc due to the Laplace force is partly transmitted to the ambient air. However, the norm of the velocity is relatively small (maximum of $0.25\,\mathrm{m\,s^{-1}}$) and mainly directed upwards, which means that the dominant effect on a large scale is the convection due to temperature gradients. The heating of the gas within the boundary layer could be interesting for flow control as it locally alters the gas viscosity and density. Furthermore, the use of a moving arc allows one to extend the heating zone to a much larger area. Compared with a steady arc actuator, the increase in the actuation zone could lead to an improvement of the arc authority on an external airflow. Moreover, the fact that the arc is covering a large area allows one to mount it on an aerodynamic system with some tolerance in its position. The zone of actuation being enlarged, the glidarc could be operated in various airflow conditions.

When the PIV system is focused on a narrower region (20 mm over the arc) and triggered on the arc ignition further information is accessible. Four phased locked acquisitions are represented in figure 10. The PIV fields are calculated from 150 snapshots taken at 0.4 Hz. The electrical excitation of the discharge and all other geometric parameters are unchanged. The first vector field is obtained when the camera opening is triggered 2 ms after the arc breakdown and the following PIV fields are obtained at $t = 4\,\mathrm{ms}$, $t = 6\,\mathrm{ms}$ and $t = 8\,\mathrm{ms}$. The left column represents the norm of the velocity vector, the middle column represents the velocity component along the x axis and the rightmost column the velocity component along the z axis.

2 ms after the ignition of the arc a small region in front of the arc with a maximum velocity of approximately $1\,\mathrm{m\,s^{-1}}$ is noticeable. The velocity in front of the arc (at $x = -10\,\mathrm{mm}$) is directed from the right to the left in the x direction and upwards in the z direction. As seen on the fields for U_x and U_z, this region of maximum velocity exhibits vectors components of $U_x = 0.7\,\mathrm{m\,s^{-1}}$ and $U_z = 0.9\,\mathrm{m\,s^{-1}}$. This

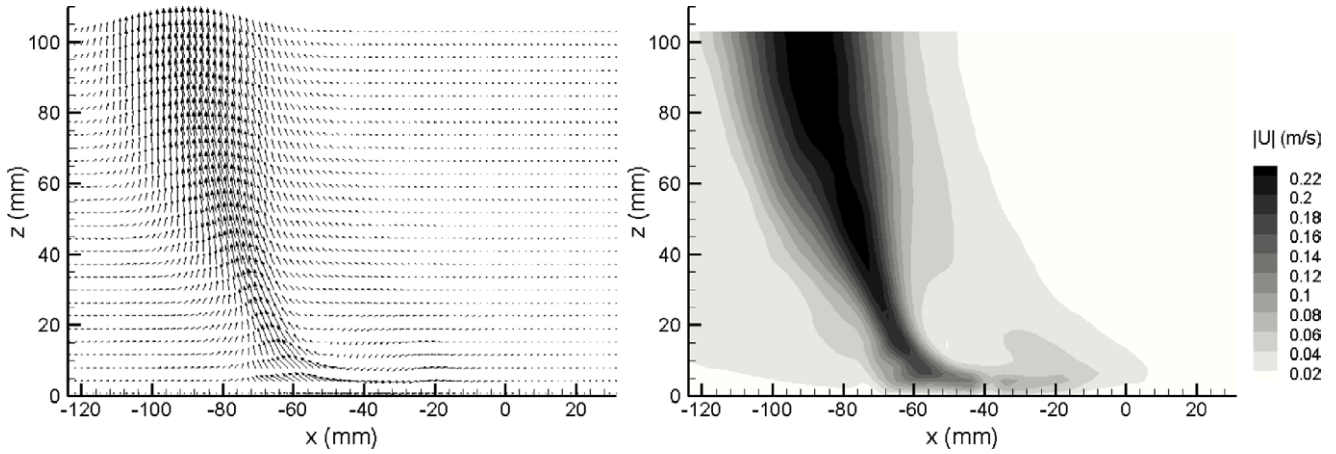

Figure 9. Average velocity field.

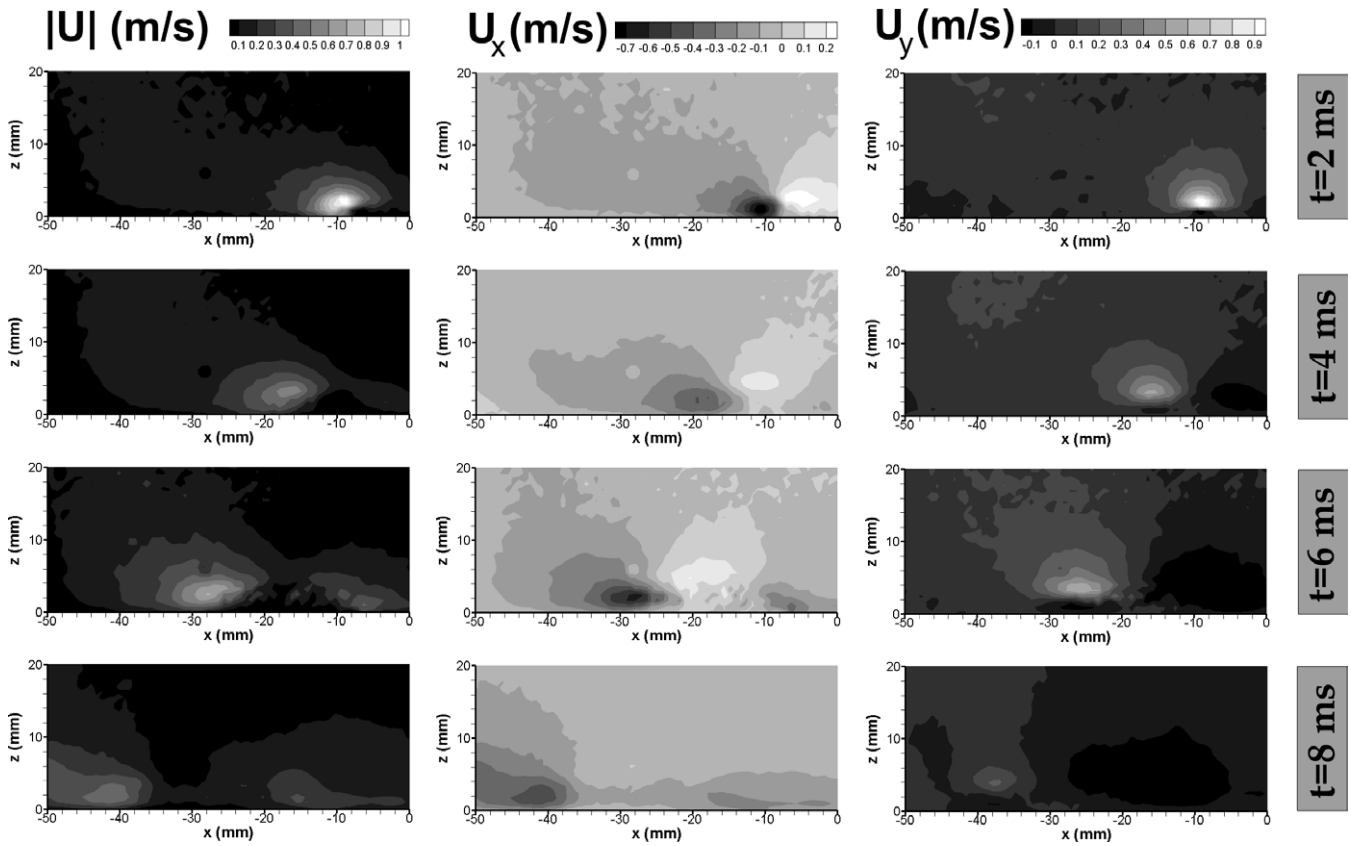

Figure 10. PIV field for the triggered case at $t = 2$ ms, $t = 4$ ms, $t = 6$ ms and $t = 8$ ms after the arc ignition.

means that at this location (2 mm above the surface and directly in front of the arc) the perturbation imparted to the air is almost equally distributed in the x and z directions. After 4 ms a similar behaviour is observed, the zone of maximal velocity follows the displacement of the arc and is mainly directed towards the left. The thermal convection is still visible and its value remains almost constant (maximum of $0.8\,\mathrm{m\,s^{-1}}$). After 6 ms the phenomenon continues as the arc is moving to the left. The zone of maximum velocity seems to have an invariant shape and the maximum values of U_x ($0.6\,\mathrm{m\,s^{-1}}$) and U_z ($0.8\,\mathrm{m\,s^{-1}}$) are almost constant. The displacement of the zone is not perfectly regular between $t = 2$ ms and $t = 6$ ms. This is certainly due to the attachment of the arc foot on the cathode mentioned earlier. After 8 ms the arc is approximately situated at $x = 36$ mm, which coincides with the zone of strong velocity observed by PIV. The component along z, U_z is positive in front of the arc (left side) and negative behind the arc (right side). This indicates that a slow airflow (lower than $0.2\,\mathrm{m\,s^{-1}}$) directed downwards exists at the back of the arc. This remarkable phenomenon could be attributed to a recirculation structure that would circle around the arc.

The mechanisms of the local interaction observed with phased locked PIV focused on the arc vicinity contrast with the overall effect of the discharge which mainly involves thermal

gradients existing on a large scale. The observation of the local perturbations proves that the glidarc not only acts on the gas by thermal effects but also creates a local gas motion in the direction parallel to its displacement and close to the wall. This is particularly interesting for boundary layer manipulations. Indeed, the glidarc could affect the state of a boundary layer (laminar, turbulent or transitional) and then be used for flow separation or reattachment in aeronautic applications or in other configurations where a controllable moving heat source is needed.

6. Conclusion

The properties of a low current arc experiencing the Laplace force in the absence of external airflow have been investigated in order to assess its possible applications to airflow control. Compared with localized fixed arcs the continuous motion of the glidarc over a 70 mm × 10 mm area prevents the surface and the electrodes from overheating. Despite the arc attachment on the cathode surface, its velocity reaches approximately 4 m s^{-1} with a current limited to 30 mA and is relatively homogeneous.

A PIV was used to observe the perturbation created by the glidarc on the surrounding air. The glidarc operates an electromagnetohydrodynamic (EMHD) conversion due to the sudden gas heating generating temperature gradients which result in gas expanding and convecting regions. When the PIV system is phased locked on the arc ignition it is possible to observe the spatio-temporal evolution of the perturbation, thereby allowing a deeper understanding of the phenomenon. It appears that in addition to the gas heating the displacement of the glidarc also results in a local gas motion parallel to its direction.

The glidarc effects on the surrounding air can probably be enhanced by increasing the magnetic field intensity and the current amplitude. The enlargement of the transfer zone with longer magnets and electrodes could also play a role in the electromechanical conversion. The excitation frequency and signal shape (square and sawtooth) should also be considered as controlling parameters that can be adjusted to maximize the electromechanical effect. In order to further evaluate the possibilities of the gliding arc in aeronautic applications we are currently investigating the mutual influence of the arc on an external airflow of a tenth of m s^{-1}.

References

[1] Roth J R, Nourgostar S and Bonds T A 2007 The one atmosphere uniform glow discharge plasma (OAUGDP)—a platform technology for the 21st century *IEEE Trans. Plasma Sci.* **35** 233–50

[2] Leonov S B, Yarantsev D A and Soloviev V R 2007 Experiments on control of supersonic flow structure in model inlet by electrical discharges *AIAA Paper 2007-3890*

[3] Macheret S O, Shneider M N and Miles R B 2004 Magnetohydrodynamic and Electrohydrodynamic control of hypersonic flows of weakly ionized plasmas *AIAA J.* **42** 7

[4] Post M L and Corke T C 2004 Separation control on high angle of attack airfoil using plasma actuators *AIAA J.* **42** 11

[5] Samimy M, Adamovich I, Webb B, Kastner J, Hileman J, Keshav S and Palm P 2004 Development and characterization of plasma actuators for high speed jet control *Exp. Fluids* **37** 577–88

[6] Moreau E 2007 Airflow control by non-thermal plasma actuators *J. Phys. D: Appl. Phys.* **40** 605–36

[7] Corke T C and Post M L 2005 Overview of plasma flow control: concepts, optimization and applications *AIAA Paper 2005-563*

[8] Benard N, Braud P, Jolibois J and Moreau E 2008 Airflow reattachment along a NACA 0015 airfoil by a surface dielectric barrier discharge actuator: time-resolved particle image velocimetry investigation *AIAA Paper 2008-4202*

[9] Post M L and Corke T C 2006 Separation control using plasma actuators: dynamic stall vortex control on oscillating airfoil *AIAA J.* **44** 3125–35

[10] Göksel B, Greenblatt D, Rechenberg I, Nayeri C N and Paschereit C O 2006 Steady and unsteady plasma wall jets for separation and circulation control *AIAA Paper 2006-3686*

[11] Corke T C, Jumper E J, Post M L, Orlov D M and McLaughlin T E 2002 Applications of weakly-ionized plasmas as wing flow-control devices *AIAA Paper 2002–0350*

[12] Sosa R, Moreau E, Touchard G and Artana G 2007 Stall control at high angle of attack with plasma sheet actuators *Exp. Fluids* **42** 143–67

[13] Jolibois J, Forte M and Moreau E 2008 Application of an AC barrier discharge actuator to control airflow separation above a NACA 0015 airfoil: optimization of the actuation location along the chord *J. Electrost.* (available online)

[14] Thomas F O, Kozlov A and Corke T C 2008 Plasma actuators for cylinder flow control and noise reduction *AIAA J.* **46** 1921–31

[15] Artana G, Sosa R, Moreau E and Touchard G 2003 Control of the near-wake flow around a circular cylinder with electrohydrodynamic actuators *Exp. Fluids* **35** 580–8

[16] McLaughlin T E, Munska M D, Vaeth J P, Dauwalter T E, Goode J R and Siegel S G 2004 Plasma-based actuators for cylinder wake vortex control *AIAA Paper 2004-2129*

[17] Font G I 2004 Boundary layer control with atmospheric plasma discharges *AIAA Paper 2004-3574*

[18] Jukes T N, Choi K S, Jonhson G A and Scott S J 2004 Turbulent boundary layer control for drag reduction using surface plasma *AIAA Paper 2004-2216*

[19] Borghi C A, Cristofolini A, Carraro M and Neretti G 2006 An analysis of a three phase flat panel uniform barrier discharge at atmospheric pressure *AIAA Paper 2006-3380*

[20] Opaits D F, Roupassov D V, Starikovskaia A Y, Zavialov I N and Saddoughi S G 2005 Plasma control of boundary layer using low-temperature non equilibrium plasma of gas discharge *AIAA Paper 2005-1180*

[21] Utkin Y G, Keshav S, Kim J-H, Kastner J, Adamovich I V and Samimy M 2007 Development and use of localized arc filament plasma actuators for high speed flow control *J. Phys. D: Appl. Phys.* **40** 685–94

[22] Zaidi S H, Smith T, Macheret S and Miles R B 2007 Snowplow surface discharge in magnetic field for high speed boundary layer control *AIAA Paper 2006-1006*

[23] Kim J H and Samimy M 1999 Mixing enhancement via nozzle trailing edge modifications in a high speed rectangular jet *Phys. Fluids* **11** 2731

[24] Samimy M, Kim J, Kastner J, Adamovich I and Utkin Y 2007 Active control of high-speed and high-Reynolds-number jets using plasma actuators *J. Fluid Mech.* **578** 305–30

[25] Samimy M, Kim J-H, Kastner J and Adamovich I 2007 Noise mitigation in high speed and high reynolds number jets using plasma actuators *AIAA Paper 2007-3622*

[26] Macheret S, Shneider M and Miles R 2003 Optimum performance of electron beam driven MHD generators for scramjet inlet control *AIAA Paper 2003-3763*

[27] Macheret S, Shneider M and Miles R 2002 Magnetohydrodynamic control of hypersonic flows and scramjet inlets using electron beam ionization *AIAA J.* **40** 74–81

[28] Risacher A, Larigaldie S, Bobillot G, Marcellin J and Picard L 2007 Active stabilization of low-current arc discharges in atmospheric-pressure air *Plasma Sources Sci. Technol.* **16** 200–9

[29] Swierczynski B, Gonzalez J J, Teulet P, Freton P and Gleizes A 2004 Advances in low-voltage circuit breaker modeling *J. Phys. D: Appl. Phys.* **37** 595–609

[30] Czernichowski A 1994 Gliding arc applications to engineering and environment control *Pure Appl. Chem.* **66** 1301–10

[31] Benstaali B, Boubert P, Chéron B G, Addou A and Brisset J-L 2002 Density and rotational temperature measurements if the NO and OH radicals produced by a gliding arc in humid air and their interaction with aqueous solutions *Plasma Chem. Plasma Process* **22** 553–71

[32] Burlica R, Kirkpatrick M J, Finney W C, Clark R J and Locke B R 2004 Organic dye removal from aqueous solution by glidarc discharges *J. Electrost.* **62** 309–21